



## Research Article

## Superhydrophobic self-extinguishing cotton fabrics for electromagnetic interference shielding and human motion detection

Lei Liu<sup>a</sup>, Zhewen Ma<sup>b</sup>, Menghe Zhu<sup>a</sup>, Lina Liu<sup>b,\*</sup>, Jinfeng Dai<sup>b</sup>, Yongqian Shi<sup>c</sup>, Jiefeng Gao<sup>d</sup>, Toan Dinh<sup>e,f</sup>, Thanh Nguyen<sup>e,f</sup>, Long-Cheng Tang<sup>g</sup>, Pingan Song<sup>e,h,\*\*</sup>

<sup>a</sup> College of Environment and Safety Engineering, Qingdao University of Science and Technology, Qingdao 266061, China

<sup>b</sup> School of Chemistry and Materials Engineering, Zhejiang A&F University, Hangzhou 311300, China

<sup>c</sup> College of Environment and Safety Engineering, Fuzhou University, Fuzhou 350116, China

<sup>d</sup> School of Chemistry and Chemical Engineering, Yangzhou University, Yangzhou 225002, China

<sup>e</sup> Centre for Future Materials, University of Southern Queensland, Springfield 4300, Australia

<sup>f</sup> School of Engineering, University of Southern Queensland, Springfield 4300, Australia

<sup>g</sup> College of Material, Chemistry and Chemical Engineering, Key Laboratory of Organosilicon Chemistry and Material Technology of MoE, Hangzhou Normal University, Hangzhou 311121, China

<sup>h</sup> School of Agriculture and Environmental Science, University of Southern Queensland, Springfield 4300, Australia

## ARTICLE INFO

## Article history:

Received 29 April 2022

Revised 28 May 2022

Accepted 30 May 2022

Available online 17 June 2022

## Keywords:

Cotton fabric

Super-hydrophobicity

Flame retardancy

Electromagnetic interference shielding

Motion sensor

MXene

## ABSTRACT

Multifunctional intelligent fire-safe cotton fabric promises next-generation fire-fighting uniform and sensor applications. However, cotton fabrics' hygroscopicity and intrinsic flammability significantly impede their potential applications in industries. Herein, we report a superhydrophobic fireproof cotton fabric (PEI-APP-PEI-MXene) generated via sequential layer-by-layer deposition of polyethyleneimine (PEI), ammonium polyphosphate (APP), and titanium carbide (MXene), followed by hydrophobic treatment with silicone elastomer. Compared to untreated cotton, the treated cotton fabric with 10 polymolecular layers exhibits ~43% and ~42% reductions in the peak heat release rate and total heat release, respectively, a desired UL-94 V-0 rating, and a high limiting oxygen index (LOI) value of 39.5 vol.%. In addition to that, the treated fabrics displayed improved electromagnetic interference (EMI) shielding and motion-sensing abilities. The presented work provides a facile and effective surface modification approach to generate multifunctional cotton fabrics with promising practical applications.

© 2022 Published by Elsevier Ltd on behalf of The editorial office of Journal of Materials Science & Technology.

## 1. Introduction

Cotton fabrics display a wide range of properties, including heat retention, biodegradability, and lightweight properties, making them desirable in clothing, packaging, and medicinal applications [1]. The advancement of intelligent technology contributes to severe electromagnetic pollution due to the necessity of electronic devices in everyday life [2,3]. For example, electromagnetic waves could interfere with the function of other electronic equipment located in its surroundings. Therefore, long-term electromagnetic radiation presents potential health and safety hazards [4,5]. The multifunctional intelligent textiles promote the rapid development of wearable technologies with inherent flexibility, monitoring

sensors, and electromagnetic interference (EMI) shielding functions [6,7]. Unfortunately, cotton fabrics with a low limiting oxygen index (LOI) value of 19 vol.% suffer from intrinsic flammability, significantly hindering their applications in stringent fire protection scenarios [8]. Another drawback to the widespread use of intelligent textiles is hygroscopicity, increasing their vulnerability to sensor functions and decreasing durability [9].

Recently, extensive efforts have been devoted to developing flame-retardant cotton fabrics while maintaining their inherent properties, such as softness and permeability. In general, commonly used modification methods for improving the flame retardancy of cotton fabrics include the sol-gel [10–14], chemical grafting [15], nanoparticle adsorption [16], and layer-by-layer self-assembly (LbL) methods (dip coating, spray coating, and vapour coating) [17–22]. For the last decade, LbL has emerged as an effective method for fabricating flame-retardant coatings on various fabrics due to its convenience and flexible assembly process. Hu and coworkers employed ammonium polyphosphate (APP), and  $Ti_3C_2T_x$  to treat cotton fabrics via the LbL dip-coating method,

\* Corresponding author.

\*\* Corresponding author at: Centre for Future Materials, University of Southern Queensland, Springfield 4300, Australia.

E-mail addresses: [liulina198310@126.com](mailto:liulina198310@126.com) (L. Liu), [pingan.song@usq.edu.au](mailto:pingan.song@usq.edu.au), [pingansong@gmail.com](mailto:pingansong@gmail.com) (P. Song).

which led to an LOI value of 36.5 vol.% [23]. Wang and coworkers presented a novel eco-friendly biomass-based coating for cotton fabrics by employing biomass tannins (TA), emetic tartar (TE), and  $\text{Fe}^{2+}$  as flame retardants [24]. However, most of the flame retardants assembled by LbL cannot withstand repeated water washing due to their inherent hydrophilicity, such as MXene, graphene oxide, and APP [25]. Therefore, the subsequent hydrophobic treatment of the assembled material is of great importance [26,27].

The unique properties of recently emerged 2D nanomaterial MXene include high electrical conductivity, high aspect ratio, and the presence of abundant surface functional groups [28]. Therefore, presenting MXene as a potential candidate in catalysis [29,30], EMI shielding [31–34], intelligent sensor [35], and flame retardancy [36–38] applications. For instance, Sun et al. developed highly conductive MXene@polystyrene nanocomposites via an electrostatic assembly approach that exhibited excellent EMI shielding performances [39]. In another study by Hu and coworkers provided a MXene-coated flame retardant cotton fabric composite for EMI shielding applications, which could reach 31.04 dB [23]. Wang et al. fabricated a highly conductive, hydrophobic, and flexible MXene-decorated poly(ethylene terephthalate) (PET) textiles with exceptional EMI shielding performance via an efficient and scalable dip-coating approach [40]. Furthermore, the deformability of knitted fabrics allows them as an ideal carrier for the fabrication of wearable strain sensors due to the unique loop fabric structure. Although such wearable MXene-decorated fibres or textiles for EMI shielding and monitoring sensor applications exhibit superior performance and maintainable inherent properties, they suffer from significant performance loss after multiple water washes and cannot meet the requirements of washable fabrics. Thus, there has been a strong demand for improving the flame retardancy and superhydrophobicity of intelligent cotton fabrics.

The presented work aims to endow cotton fabrics with flame retardancy, superhydrophobicity, EMI shielding, and motion-sensing functions. A facile, eco-friendly, and LbL self-assembly route was adopted by cyclically depositing polyethyleneimine (PEI), APP, PEI, and MXene solutions. PEI is an ideal cationic polyelectrolyte for LbL assembling, benefiting from its advantages of non-toxic and water-soluble properties. APP is a common flame retardant that can serve as an anionic polyelectrolyte. Whereas, negatively charged MXene nanosheets are used as special functional substances due to their electrical conductivity and physical barrier properties. This water-based PEI-APP-PEI-MXene coating combined with an ultra-thin silicone elastomer layer impart self-extinguishing, good EMI shielding, sensor monitoring, and superhydrophobic performance cotton fabrics with only ten polymolecular layers. Additionally, the peak heat release rate (PHRR) and total heat release (THR) are reduced by 43% and 42%, respectively. Compared to previous studies (such as FC-5.2Ti<sub>3</sub>C<sub>2</sub>T<sub>x</sub> [23] and PTFRF1.2 [41]), the as-prepared sample cotton-10BL-Si with motion sensor function shows a higher limiting oxygen value of 39.0 vol.%, a higher initial degradation temperature (increased by 21 °C), superhydrophobicity, and washability. This work provides an innovative strategy for multifunctional cotton fabrics with good flame retardancy, thermal stability, and durability, holding promise for their practical application in electronics, construction, military, and other fields.

## 2. Experimental

### 2.1. Materials

Cotton fabrics (100%, 315 g/m<sup>2</sup>) were purchased from the Yifang Textiles Co., China. Polydimethylsiloxane (PDMS, silicone elastomer-184) and curing agent (curing agent-184) were purchased from Dow-Corning Co., Ltd. Ammonium polyphosphate

(APP, phase II, the degree of polymerization >1000) was provided by Hangzhou JLS Co., Ltd. Polyethyleneimine (PEI,  $M_w = 10,000$ ) was provided by Aladdin Chemicals Co., Ltd. The Ti<sub>3</sub>AlC<sub>2</sub> (powders, 99% purity) were provided by 11 Technology Co., Ltd. Hydrochloric acid (HCl, 37%) and lithium fluoride (LiF) were supplied by Sinopharm Chemical Reagent Co., Ltd.

### 2.2. Synthesis of MXene

Ti<sub>3</sub>AlC<sub>2</sub> (0.5 g) is mixed with 0.5 g of LiF in the presence of HCl solution (10 mL, 12 mol/L) under magnetic stirring. The mixture is stirred at 40 °C for 24 h followed by repeated washing with deionized water. The sediment in 100 mL of deionized water is then ultrasonicated for 30 min in an ice bath. Finally, the resultant MXene nanosheets are collected via centrifugation at 9000 rpm for 5 min.

### 2.3. Fabrication of cotton fabrics by LbL deposition

The cotton fabric is first boiled in NaOH solution to remove the grease on its surface and then dried in an oven at 80 °C for 24 h. Then, cotton fabric is immersed in the PEI solution (4 mg/mL) for 3 min to deposit a PEI layer. After washing with DI water, the PEI-coated sample is then immersed into an APP solution (20 mg/mL) for 3 min, followed by washing with DI water and immersing in the PEI solution. Subsequently, the PEI/APP/PEI-coated sample is immersed in an MXene solution (2 mg/mL) to get a MXene layer. This coating process of PEI/APP/PEI/MXene layers is recycled 3, 5, and 10 times. Finally, the coated fabric is dried at 60 °C in a vacuum oven to remove the residual water.

### 2.4. Superhydrophobic treatment of cotton fabrics

40 g PDMS and 4 g curing agent (weight ratio is 10:1) are first dissolved in 200 mL n-hexane to give ~10% (w/w) polymer solution. Subsequently, the cotton fabric is immersed in the above solution for 7 min. Thereafter, the treated cotton fabrics are cured in an oven at 80 °C for 1 h, and the superhydrophobic samples with PDMS surface are obtained.

### 2.5. Characterization

Infrared (IR) spectra are recorded on a Bruker Vector 22 FTIR instrument using an attenuated total reflectance (ATR) mode. X-ray photoelectron spectrometer (XPS) is measured by a Thermo ESCALAB 250XI instrument with K-alpha radiation X-rays at 300 W. X-ray diffractions (XRD) analysis is conducted on an X-ray diffractometer (Rigaku Co., Japan) with Cu K $\alpha$  radiation at 40 kV. Scanning electron microscope and energy dispersive X-ray spectrometry (SEM-EDS) images are obtained using a SU8010 instrument. Transmission electron microscopy (TEM) observations are performed using JEOL JEM2011 equipment. The water contact angle (WCA) and the sliding angle are determined by a SL200KS Dynamic/Static Optical Contact Angle Meter (Solon Tech. Co., Ltd., China).

Thermogravimetric analyzer coupled with Fourier transform infrared spectroscopy (TG-IR) is carried out with a thermogravimetric analyzer (DT-50) and a FTIR spectrometer (170SX) from 40 to 800 °C at a heating rate of 10 °C/min under nitrogen atmosphere. The sample weight is in the range of 5–10 mg. The UL-94 vertical burning test is performed on a CZF-3 vertical burning tester according to the ASTM D3801 standard. LOI is performed using an oxygen index analyzer (Fire Testing Technology, UK) according to the ASTM D2863-09 standard. The MCC measurement is conducted on a pyrolysis combustion flow calorimeter (Stanton Redcroft, UK) according to the ASTM D7309 standard.

The electrical conductivity is measured with a four-point probe (FT-340, Ningbo ruike Co., Ltd, China) via the standard four-point contact method. The resistivity signals of sample fabrics are

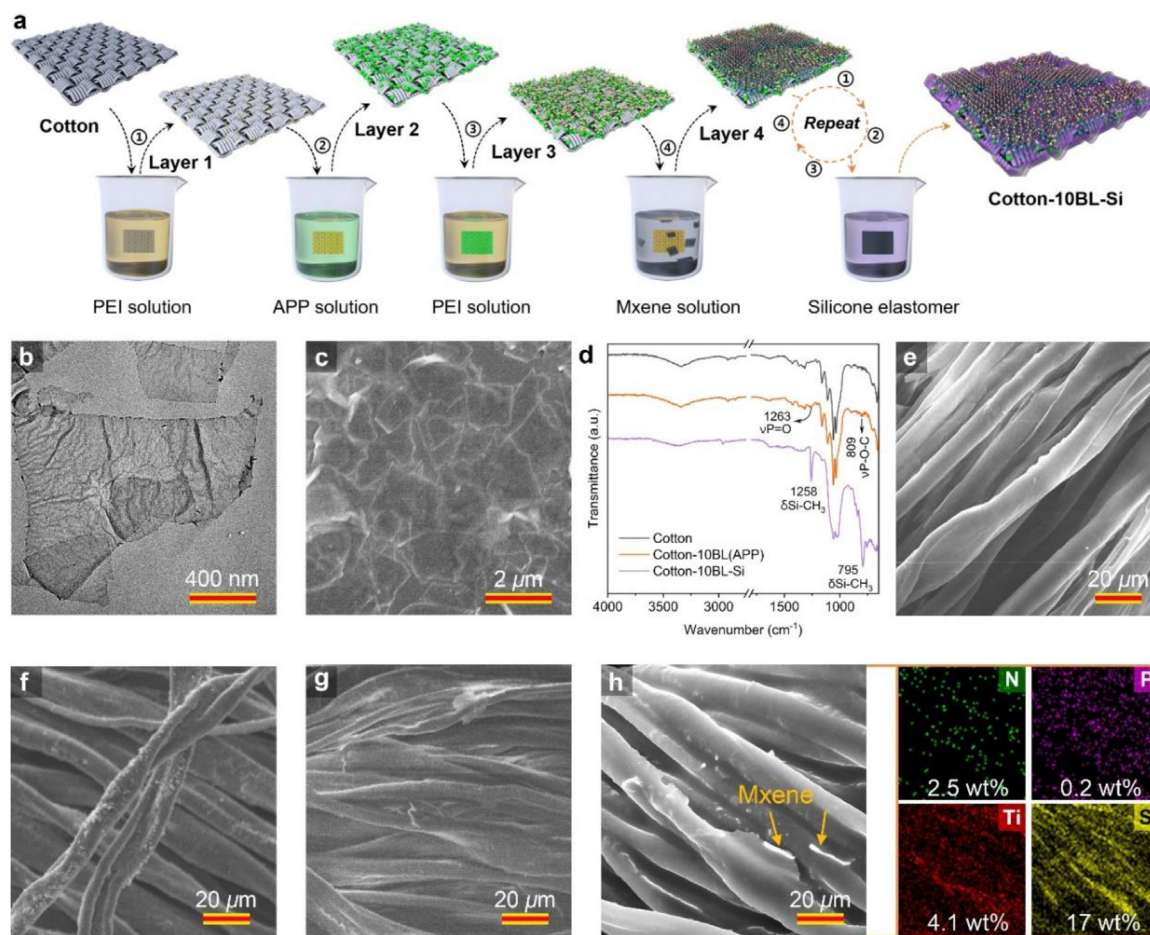


**Fig. 1.** Schematic illustration for layer-by-layer self-assembly treatment and characterization of multifunctional cotton fabrics. (a) Illustration of LbL treatment to cotton fabrics; (b) TEM image of MXene; (c) SEM image of MXene; (d) IR spectra of cotton and coated cotton; SEM images of (e) cotton, (f) cotton-5BL-Si, and (g) cotton-10BL(APP)-Si; (h) SEM image of cotton-10BL-Si along with the EDS mapping results.

recorded by a digital multimeter (Keithley DMM7510). A vector network analyzer (AV3672) in the 8.2–12.4 GHz region was used to record the electromagnetic interference shielding data of sample fabrics. When the electromagnetic waves hit the shielding material, the reflection coefficient ( $R$ ), transmission coefficient ( $T$ ), and the absorption coefficient ( $A$ ) are expressed as:

$$S_{11} = 10 \lg R \quad (1)$$

$$S_{21} = 10 \lg T \quad (2)$$

$$R = 10^{(S_{11}/10)} \quad (3)$$

$$T = 10^{(S_{21}/10)} \quad (4)$$

$$A = 1 - R - T \quad (5)$$

The total shielding effectiveness ( $SE_T$ ) consists of the absorption SE ( $SE_A$ ), reflection SE ( $SE_R$ ), and multiple internal reflection SE ( $SE_M$ ), given by the equation:

$$SE_T = SE_R + SE_A + SE_M \quad (6)$$

$$SE_R = -10 \lg(1 - R) \quad (7)$$

$$SE_A = -10 \lg(T/(1 - R)) \quad (8)$$

The accelerated wash durability test of sample fabrics is conducted according to AATCC 61–2006 standard. The sample is washed in a 550 mL stainless steel container at 49 °C for 45 min with a rotation speed of 40 rpm, which also contains 50 stainless steel balls and 150 mL of 0.15% detergent solution.

### 3. Results and discussion

#### 3.1. Fabrication of PEI/APP/PEI/MXene coating on cotton fabric

The schematic of the design strategy of cotton-10BL-Si is represented in Fig. 1(a). Cotton fabric was first pretreated by PEI solution through a facile impregnation process. PEI, a commercially available water-soluble polymer and a common flame retardant, is decorated onto the surface of hydrophilic cotton fabric via interfacial hydrogen bonding interaction [42]. Due to the electrostatic attraction between PEI and APP, the negatively charged APP is subsequently selected as one of the building blocks, which acts as a flame retardant in both gaseous and condensed phases. Similarly, MXene nanosheets as another negatively charged building block can also assemble onto the PEI coating surface. Therefore, cotton fabrics can be fabricated by sequential layer-by-layer deposition of PEI-APP-PEI-MXene. Benefiting from the high electrical conductivity and two-dimensional lamellar structure of MXene and the synergistic flame retardancy of MXene and APP, the PEI-APP-PEI-MXene-coated cotton fabrics also demonstrate the versatility and high fire safety. The last step of the silicone elastomer package en-

dows the fabrics with superhydrophobicity, long-lasting fire resistance, and washability even after the repeated washing process.

### 3.2. Morphology and microstructure

SEM and TEM analysis are used to investigate the morphological features of MXene (Fig. 1(b)). The exfoliated MXene nanosheets exhibit nearly transparency under electron beams, with the presence of certain folding and twisting structures, indicating that the exfoliated ultra-thin nanosheets are obtained [43]. Meanwhile, it exhibits a typical two-dimensional lamellar structure (Fig. 1(c)) with a lateral size from 400 to 1,600 nm. XRD pattern of MXene shows a sharp and strong diffraction peak at  $2\theta = 6.2^\circ$  belonging to the (002) phase (Fig. S1(a) in Supplementary Material). XPS is performed to further investigate the chemical compositions and bond types of MXene. MXene shows binding energy (BE) peaks at 461.4 eV (Ti 2p<sub>1</sub>), 455.6 eV (Ti 2p<sub>3</sub>), and 284.8 eV (C 1s) (Fig. S1(b–d)). To confirm that multilevel PEI-APP-PEI-MXene@Si coating is successfully loaded on the cotton fabrics, the chemical state, surface morphology, and the elemental composition of coated cotton fabrics are determined by IR-ATR, SEM, and EDS mapping results. Compared to untreated cotton, several new characteristic peaks of Cotton-10BL and Cotton-10BL-Si samples can be observed in IR spectra (Fig. 1(d)). The absorption peaks at 1260 and 809  $\text{cm}^{-1}$  indicate stretching vibration of the P=O and P-O-P groups from APP [44]. In addition, the appearance of two additional strong absorption peaks at 1258  $\text{cm}^{-1}$  and 795  $\text{cm}^{-1}$ , respectively, were assigned to the Si-CH<sub>3</sub> band of sample cotton-10BL-Si due to the outermost encapsulation of a silicone elastomer coating.

The SEM characterization and EDS mapping are taken to reveal the microstructure of cotton, cotton-10BL(APP)-Si, and cotton-10BL-Si (Fig. 1(e–h)). Typically, the untreated cotton fabric is composed of interwoven fibre bundles, displays a relatively smooth fibre surface at high magnifications (Fig. 1(e) and Fig. S2). Whereas cotton-5BL-Si, cotton-10BL(APP)-Si, and cotton-10BL-Si exhibit relatively rough surfaces with many random-shaped particles post multiple LbL processes, which are consisted of the overlapping PEI, APP, and MXene layers (Fig. 1(f–h)). The uniform distribution of the Ti element on its surface from the EDS mapping results (Fig. 1(h)) confirms the assembly of the MXene layer. As a result, the conductive MXene coating forms a continuous conductive path on the surface of the cotton fabric frame, which endows the fabric with exceptional EMI shielding properties and a flame-retardant shield for the inner fabric [45]. Besides, the EDS mapping images also show the homogeneous dispersion of N and P elements from APP and PEI and abundant Si elements (17 wt%) from the outermost silicone elastomer layer of the fabric (Fig. 1(h)). As shown in Fig. S2, the average thickness of 10BL-Si coating onto each fibre measured by the software ImageJ is  $\sim 4.4 \mu\text{m}$ , and the PDMS shows a negligible effect on covering the air holes between interwoven fibre bundles. So the coated fabric can still maintain its good air permeability.

### 3.3. Properties of the coated cotton fabric composites

#### 3.3.1. Surface wettability performance

Water contact angle (WCA) tests are conducted to investigate the surface wettability properties of neat cotton fabric and various sample fabrics treated with LbL coatings or additional silicone elastomer coating (Fig. 2). Typically, the water droplets can quickly penetrate the hydrophilic cotton fabric, so all-cotton fabric samples without silicone elastomer packaging exhibit WCAs of  $0^\circ$  (Fig. 2(a)), which is consistent with previously reported findings [40]. This is due to the presence of abundant hydroxyl groups on the surface of cotton fibers. It is worth mentioning here that the samples only

treated with PEI-APP or PEI-APP-PEI-MXene coatings show similar water permeability as the pure cotton, implying that all MXene and APP coating layers in this system make no contribution to the hydrophobic property. In sharp contrast, silicone elastomer encapsulation endows fabrics with superhydrophobic features with a high WCA value of  $152.9^\circ$ , which can protect MXene from oxidation or degradation in high humidity environments (Fig. 2(a–c)) [40]. Furthermore, the superhydrophobic surface also builds the foundation for multifunctional fabrics to maintain stable performance after the repeated water washing.

The self-cleaning function of cotton fabrics can significantly prevent them from being polluted in daily use. Herein, several water droplets dissolving various pigments are dropped on the Cotton-10BL-Si surface, which shows excellent antifouling performance. The self-cleaning function is also reflected by the non-diffusion of liquid droplets for a long time and maintaining a stable spherical shape on the surface (Fig. 2(d)). Furthermore, the anti-splash performance is studied, as shown in Fig. 2(d). Under the continuous impact of the water column, the cotton-10BL-Si can endure the water flow. Moreover, the surface shows resistance to water stains, demonstrating its superior self-cleaning and anti-fouling performances.

#### 3.3.2. Thermal and fire performances

As a potential multifunctional cotton fabric, assessing its thermal and fire performance is vital. Herein, TGA measurements are conducted to evaluate the thermal stability, degradation behaviour, and charring capability of sample fabrics. Fig. 3(a–c) and Table S1 summarize the data of initial degradation temperature  $T_i$  (where 5 wt% weight loss), the maximum weight loss temperature  $T_{\text{max}}$ , and the char residue at 800 °C [46]. Under nitrogen atmosphere, all samples exhibit a two-step decomposition behaviour, which is consistent with the thermal properties of the cotton itself. Pure cotton begins to decompose at 285 °C, showing two distinct stages of mass loss at 342 °C and 491 °C, respectively, with almost no residual char ( $\sim 0.7 \text{ wt}\%$ ) at 800 °C. The first step (at 300–400 °C) corresponds to the degradation of the main chains of cotton fabric with the formation of aliphatic char and volatile products. The second step (at 400–520 °C) relates to the formation of aromatic compounds, carbon mono and dioxide.

In contrast, cotton-10BL(APP)-Si exhibits a higher  $T_i$  value of 306 °C. At the same time, other samples containing MXene exhibit higher  $T_i$  but lower  $T_{\text{max-1st}}$  values, indicating the heat blocking effect of the MXene layer. In addition, the advanced thermal degradation step of APP and PEI layers leads to a decrease of the  $T_{\text{max-1st}}$  with the formation of NH<sub>3</sub> and stable heat-insulating flame retardation layers [47]. Therefore, all assembled samples exhibit much higher  $T_{\text{max-2nd}}$  values, such as Cotton-10BL-Si reaching the highest  $T_{\text{max-2nd}}$  value of 543 °C. Furthermore, after tests, all char residues of the coated samples are much higher than that of the control cotton. The increase of residual char depends on the cycle number of the LbL process, indicating the composite coating enhances the thermostability of sample fabrics at high temperatures. For instance, char residues from cotton-3BL-Si, cotton-5BL-Si, and cotton-10BL-Si at 800 °C show a 2843%, 3014%, and 3717% increase, respectively, as compared to that of neat cotton.

#### 3.3.3. Flame retardancy

A microscale cone calorimeter (MCC) measurement is conducted to investigate the fire safety of coated cotton fabrics [48]. Cotton fabrics before and after coating treatment were all heated from 100 to 500 °C at a heating rate of 1 °C/s with a nitrogen/oxygen (80/20, volume ratio) gas mixture. The representative heat release rate (HRR) and total heat release (THR) curves are shown in Fig. 3(d, e). The detailed data of peak HRR (PHRR), THR, heat release capacity (HRC), and the temperature at PHRR ( $T_{\text{PHRR}}$ )

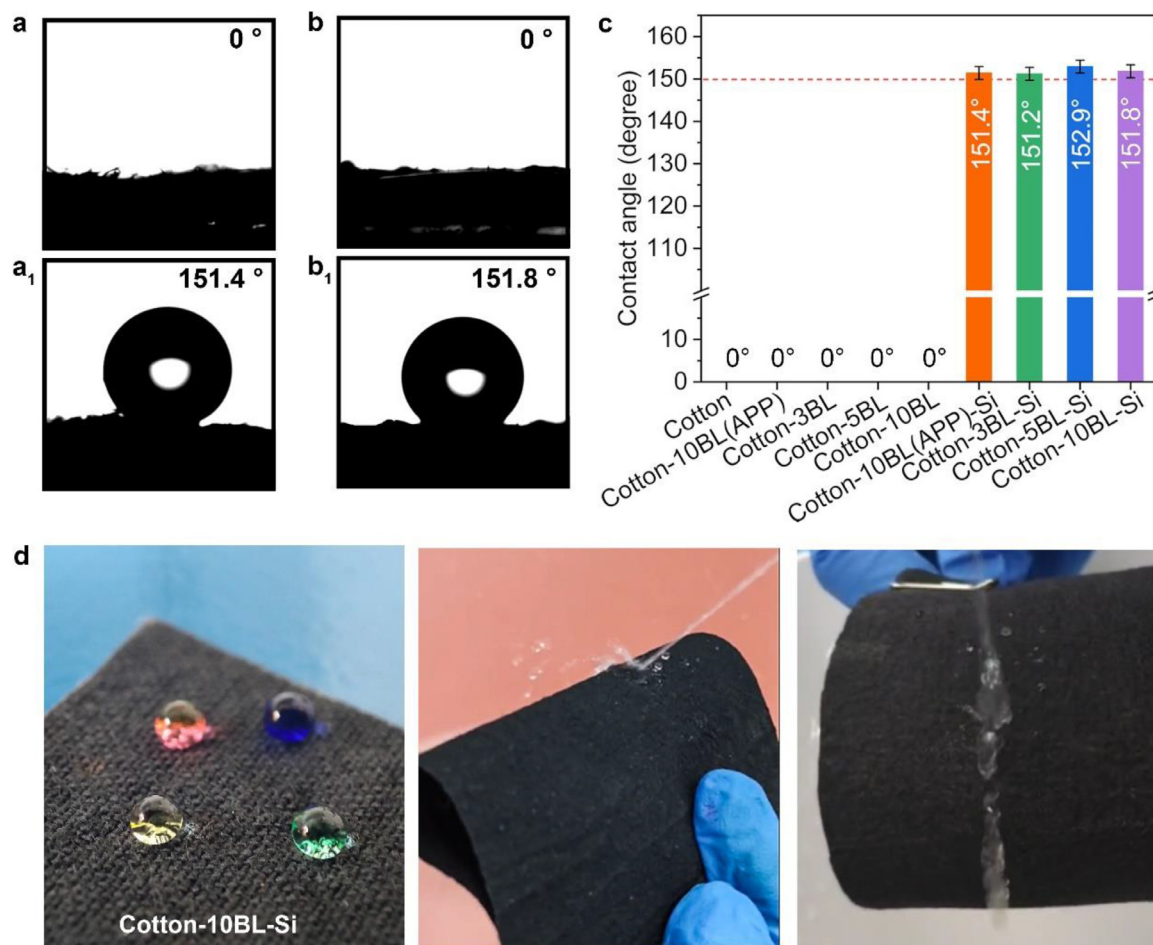


**Fig. 2.** Superhydrophobic and self-cleaning properties. Water droplets deposited on the (a) cotton-10BL(APP), (a<sub>1</sub>) cotton-10BL(APP)-Si, (b) cotton-10BL and (b<sub>1</sub>) cotton-10BL-Si; (c) WCA of all samples; (d) superhydrophobic surface property of the cotton-10BL-Si.

is summarized in Table S2. Firstly, pure cotton fabric shows a very high PHRR value of 287 W/g at a  $T_{\text{PHRR}}$  of 385 °C and a high THR value of 15.1 kJ/g due to its inherent flammability. Upon 10-BL coating of PEI-APP, both the PHRR and THR values of cotton-10BL(APP) decrease, indicating the prominent effect of the PEI-APP coating on reducing fire hazards. In addition, MXene nanosheets can further enhance the fire resistance of cotton fabrics, as evidenced by a low PHRR of 220 W/g and a THR of 9.9 kJ/g of sample cotton-3BL-Si with only 3 deposition cycles. In particular, cotton-10BL-Si gives rise to a remarkable decrease of 24% in PHRR (from 216 to 164 W/g) and a 4% reduction in THR relative to the cotton-10BL(APP)-Si, suggesting the combination or synergistic effects of APP, PEI, and MXene. The decreased temperature to PHRR ( $T_{\text{PHRR}}$ ) is caused by the thermal-oxidative degradation of APP, which can catalyze the formation of carbon layer to retard the heat transfer (Table S2).

Limiting oxygen index (LOI) and UL-94 vertical burning test are also conducted to evaluate the flammability performance of sample fabrics. Untreated cotton fabric shows a low LOI of ca. 19.0 vol% and no UL-94 ratings (Fig. 3(f) and Table S3). Upon exposure to the flame, cotton fabric can be ignited within 5 s, followed by a continuous fierce burning until burning out even after removing the ignition source (Fig. 3(g)). After testing, there were only a few residues left for untreated cotton. The flame-retardant rating of cotton fabrics is closely related to the number of Lbl cycles of composite coating (PEI-APP or PEI-APP-PEI-MXene). After more than 5 soaking cycles, the samples can reach the UL-94 V-0 rating, a necessary fire safety standard in actual production. Cotton-10BL

(APP) -Si and cotton-10BL-Si both exhibit high LOI values up to 39.0 vol.% and 39.5 vol.%, respectively, indicating the vital role of PEI-APP amounts in enhancing the flame retardancy and controlling the self-extinguishing behaviour of fabrics (Fig. 3(f) and Table S3). Thus, the flame can be extinguished immediately after torch removal (Fig. 3(h–i)) during vertical burning testing, and the tested samples still maintain their intact shape.

### 3.3.4. Fire-retardant mechanism

To reveal how PEI-APP and MXene work in the condensed phase during combustion, the residual chars generated after the vertical burning test are collected for SEM and Raman analysis. The char residue of neat cotton fabric shows a porous and loose structure, primarily consisting of elements C (40 wt%), O (41 wt%), and N (1.5 wt%) (Fig. S3(a)). In contrast, the residual char of cotton-10BL-Si exhibits an intact and compact structure without any voids (Fig. S3(b)). And the elemental mapping results show the uniform distribution of C, Ti, P, and Si elements, implying that the flame retardant can promote the formation of a superior carbonaceous layer in the condensed phase. It is worth noting that abundant element Si (38 wt%) is detected, indicating that the outer char residue largely derives from the silicone elastomer layer. The Si-rich layer prevents the underlying layers and substrate from the external flame and enhances the flame retardancy of the sample fabric. IR analysis further studies the chemical compositions of the char residues from cotton and cotton-10BL-Si. The IR spectrum of the burnt cotton fabric (Fig. S3(c)) shows several absorption peaks at 3430  $\text{cm}^{-1}$  ( $\nu_{\text{O-H}}$ ), 1079  $\text{cm}^{-1}$  ( $\nu_{\text{C-OH}}$ ), and 885  $\text{cm}^{-1}$

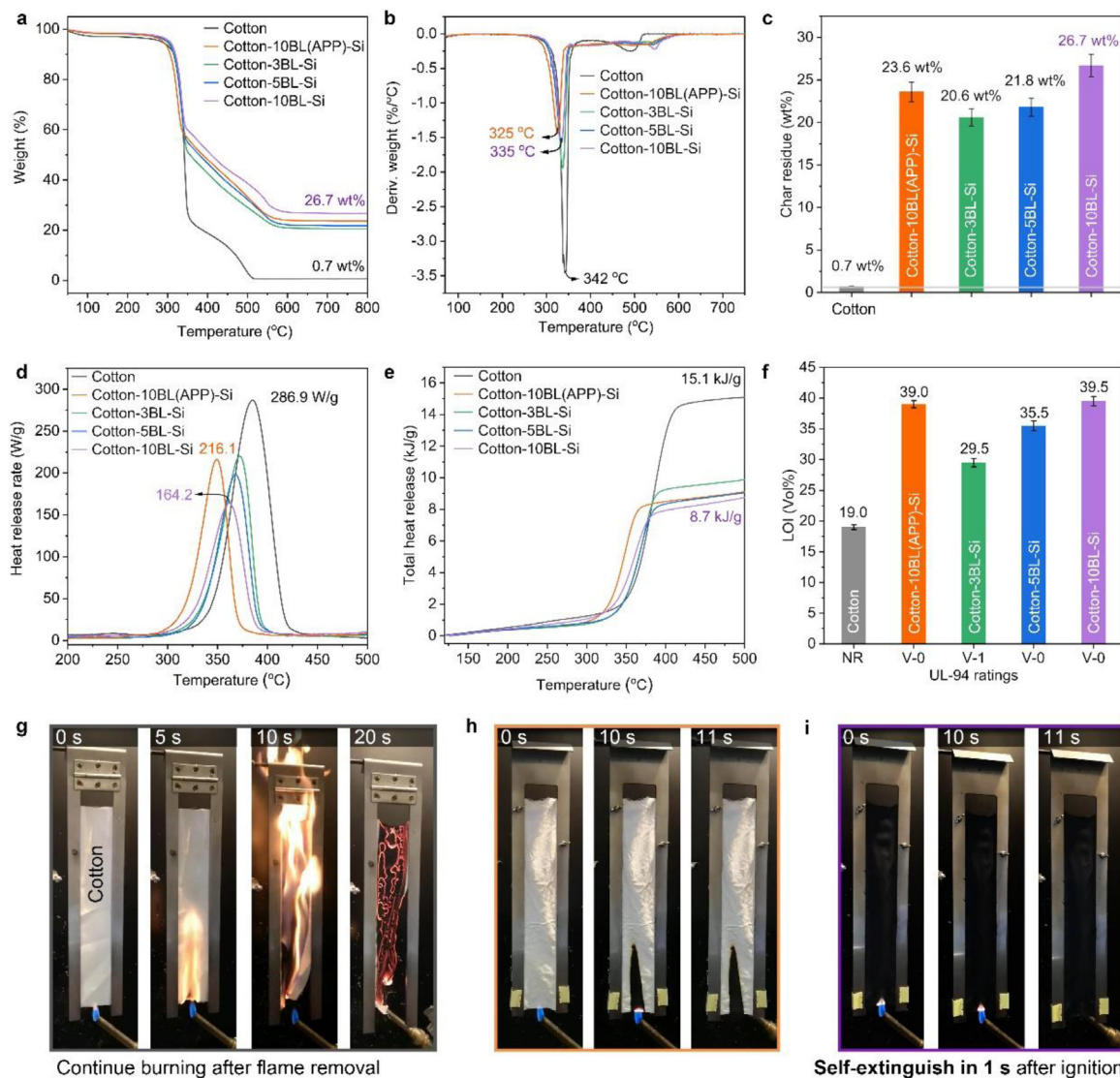


**Fig. 3.** Thermal stability and flame retardancy. (a) TGA, (b) DTG curves, and (c) char residues of cotton and coated cotton fabrics; (d) Heat release rate and (e) total heat release curves; (f) LOI values and UL-94 ratings for cotton and coated cotton fabrics; Digital photos for (g) cotton, (h) cotton-10BL(APP)-Si and (i) cotton-10BL-Si during vertical burning tests.

( $\delta\text{CH}_2=\text{CH}_2$ ) [49]. In comparison, the char residue for cotton-10BL-Si exhibits new characteristic peaks at  $1093\text{ cm}^{-1}$  (P-O-P) arising from APP, and  $1274$  and  $813\text{ cm}^{-1}$  belonging to  $\text{Si}-\text{CH}_3$  [42], agreeing well with the above SEM results, further demonstrating the condensed-phase action of APP and silicone elastomer.

Raman spectroscopy is usually employed to evaluate the quality of char residues. Two distinct characteristic peaks at about  $1396\text{ cm}^{-1}$  (D bands, representing the disordered graphite-like structures) and  $1578\text{ cm}^{-1}$  (G bands, representing ordered crystalline graphite) are detected (Fig. S3(d–g)). The graphitization degree of char residue reflects its quality, which is assessed by the intensity ratio of D and G bands ( $I_D/I_G$ ) [46]. The values of  $I_D/I_G$  of the char follows the sequence: Cotton-10BL-Si (2.46) < Cotton-10BL(APP)-Si (2.93) < Cotton-3BL-Si (3.97) < Cotton (4.19). The results show that the char of cotton-10BL-Si has the highest graphitization degree. This indicates that the presence of MXene nanosheets has influenced the graphitization transition of the coated cotton fabrics during the combustion process.

TG-IR analysis is further used to understand the thermal decomposition behavior of cotton and cotton-10BL-Si. From the 3D IR spectra, the assembly of the composite coating can dramati-

cally alter the thermal decomposition process of cotton fabric (Fig. S4(a, b)). The characteristic pyrolysis products of cotton fabrics mainly include  $\text{H}_2\text{O}$  ( $3600\text{--}3750\text{ cm}^{-1}$ ), hydrocarbons ( $2970\text{--}2811\text{ cm}^{-1}$ ),  $\text{CO}_2$  ( $2355\text{ cm}^{-1}$ ),  $\text{CO}$  ( $2181\text{ cm}^{-1}$ ), and carbonyl compounds ( $1737\text{ cm}^{-1}$ ) [50]. For cotton-10BL-Si, the absorption peak at around  $3224\text{ cm}^{-1}$  belongs to  $\text{NH}_3$  from the decomposition of APP, which can dilute the combustible compounds in the gaseous phase (Fig. S4(c)). The IR signals of major volatile products as a function of temperature are presented in Fig. S4(d–h). The lower volatile intensity of cotton 10BL-Si is due to the carbonization effect of flame retardants and the Si-rich char that can remarkably attenuate the combustion reaction; the physical barrier effect of high aspect-ratio MXene nanosheets can work synergistically to slow down the burning process and inhibit the heat and mass transfer [51–53]. For example, cotton-10BL-Si shows a weaker CO intensity and suppresses the CO release of the sample in the later stages of combustion as compared to untreated cotton fabric, suggesting the lower smoke toxicity of cotton-10BL-Si during combustion (Fig. S4(h)). Notably, the intensity peak of volatiles for cotton-10BL-Si appears earlier than pure cotton, which might be related to its advanced  $T_{\text{max}}$  (Table S1).

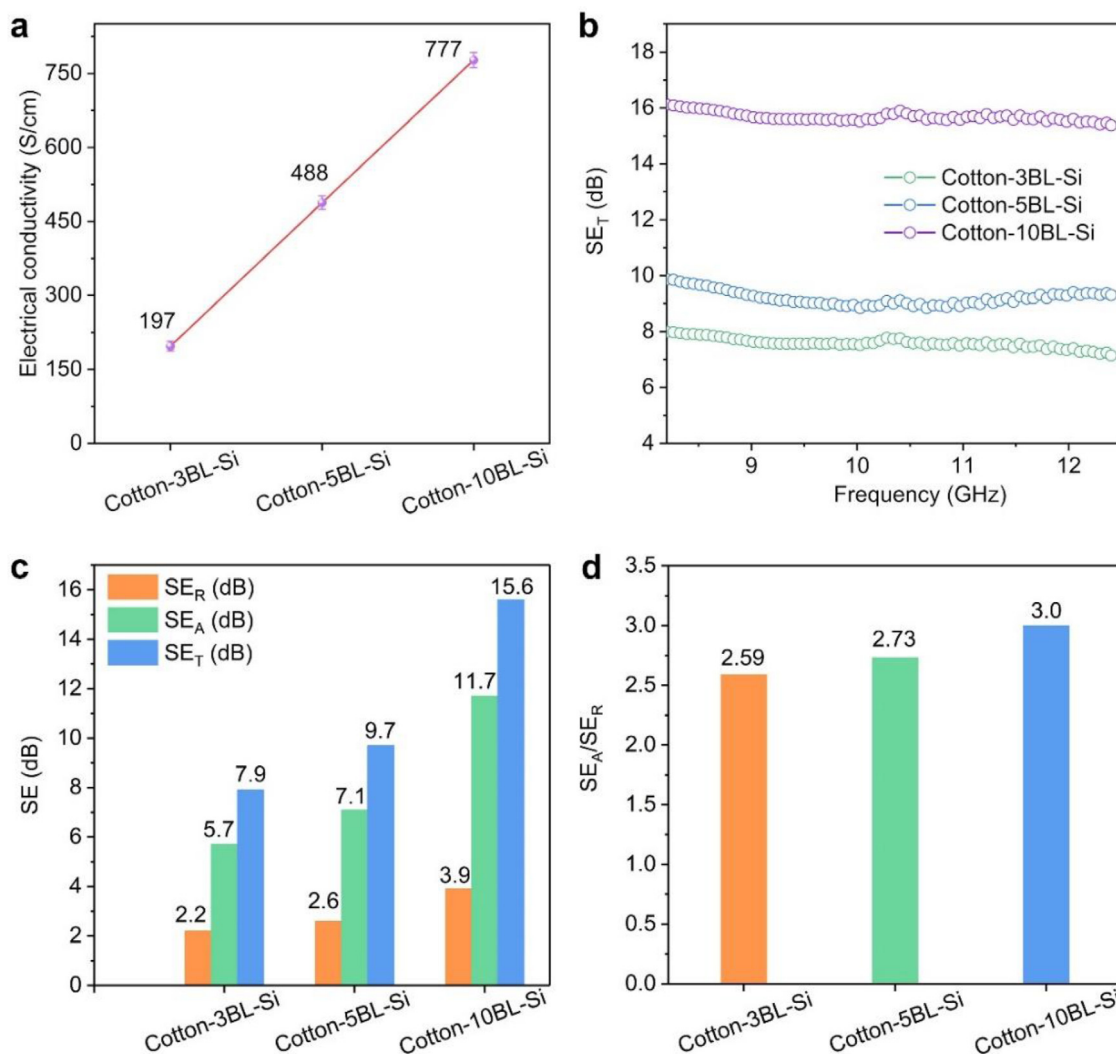


**Fig. 4.** Electrical conductivity and EMI shielding properties. (a) Electrical conductivity, and (b) EMI shielding performance of samples; (c) SE<sub>R</sub>, SE<sub>A</sub>, and SE<sub>T</sub> values of samples; (d) ratios of SE<sub>A</sub>/SE<sub>R</sub> of the samples.

Based on the above reported and experiment results, a possible flame-retardant model can be proposed to interpret the flame-retardant mechanism of coated cotton fabrics. The flame-retardant layers (PEI-APP) play a crucial role in slowing down the combustion reaction during combustion. Upon exposure to external heat flux, PEI-APP firstly degrades to promote the formation of a thermostable compact carbonaceous layer while decomposes to release inert compounds (H<sub>2</sub>O, NH<sub>3</sub>, and N<sub>2</sub>) to dilute the fuel concentrations in the gas phase. Meanwhile, the Si-rich char residue formed by the silicone elastomer layer combined with tortuous paths formed by the 2D MXene nanosheets can hinder heat and mass transfer and slow down the combustion reaction [54–56]. It can be summarised that as designed synergistic flame retardant system composed of PEI, APP, MXene, and silicone elastomer layer can fully function in the gas and condensed phases by promoting carbonization, diluting fuel, and working as a physical barrier.

### 3.3.5. Electrical conductivity and EMI shielding properties

As-prepared MXene-based materials also demonstrate good EMI shielding properties due to the good electrical conductivity of MXene [28,57]. Furthermore, the EMI shielding properties of coated cotton fabrics were evaluated by the electrical conductivity and SE measurements as represented in Fig. 4. With increasing the number of MXene layers, the electrical conductivity of the samples in-

creases remarkably (Fig. 4(a)). A high conductivity of coated fabric up to 777 S/cm is obtained after 10 LbL cycles. The prominent electrical conductivity implies obvious advantages of MXene layers in EMI shielding fabrics. The SE<sub>T</sub> of MXene coated flame-retardant cotton fabrics exhibits a weak frequency dependence (Fig. 4(b)). The large mesh macrostructures of knitted cotton fabric composites lead to a less intact and poorly conductive network on the cotton surface during a single soaking process. Therefore, satisfactory EMI SE values can only be achieved when MXene loading reaches a relatively higher level (Fig. 4b). The total EMI shielding effectiveness (SE<sub>T</sub>), microwave absorption (SE<sub>A</sub>), and microwave reflection (SE<sub>R</sub>) of the MXene coated samples are also listed in Fig. 4(c). In particular, the SE<sub>T</sub> of cotton-10BL-Si reaches the highest value of 15.6 dB, indicating a satisfying EMI shielding effect. SE<sub>T</sub> consists of SE<sub>A</sub> and SE<sub>R</sub>, and the SE<sub>A</sub> values of coated cotton fabrics are all higher than the SE<sub>R</sub> values no matter of MXene loadings (Fig. 4(c)). For instance, cotton-10BL-Si exhibits SE<sub>R</sub>, SE<sub>A</sub>, SE<sub>T</sub> values of 3.9 dB, 11.7 dB, and 15.6 dB, respectively, of which SE<sub>A</sub> value is 3 times SE<sub>R</sub> (Fig. 4(d)). The absorption coefficient (A) values of the composites film gradually decrease, whereas an opposite trend is observed for the reflection coefficient (R) values (Fig. S5). The A and R values of cotton-10BL-Si are 0.38 and 0.59, respectively, indicating that the primary EMI shielding mechanism depends on reflection although SE<sub>R</sub> is lower than SE<sub>A</sub>.

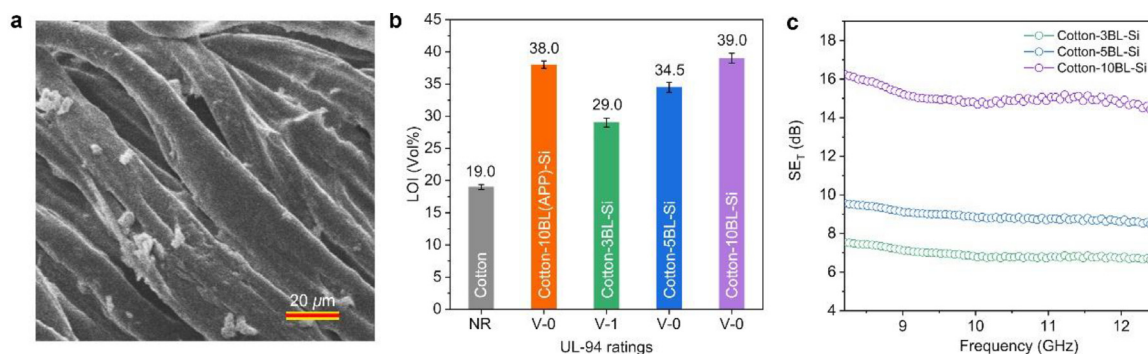


Fig. 5. The performance of the fabric after the washing. (a) SEM image of cotton-10BL-Si; (b) EMI shielding performance of samples; (c) LOI values and UL-94 ratings.

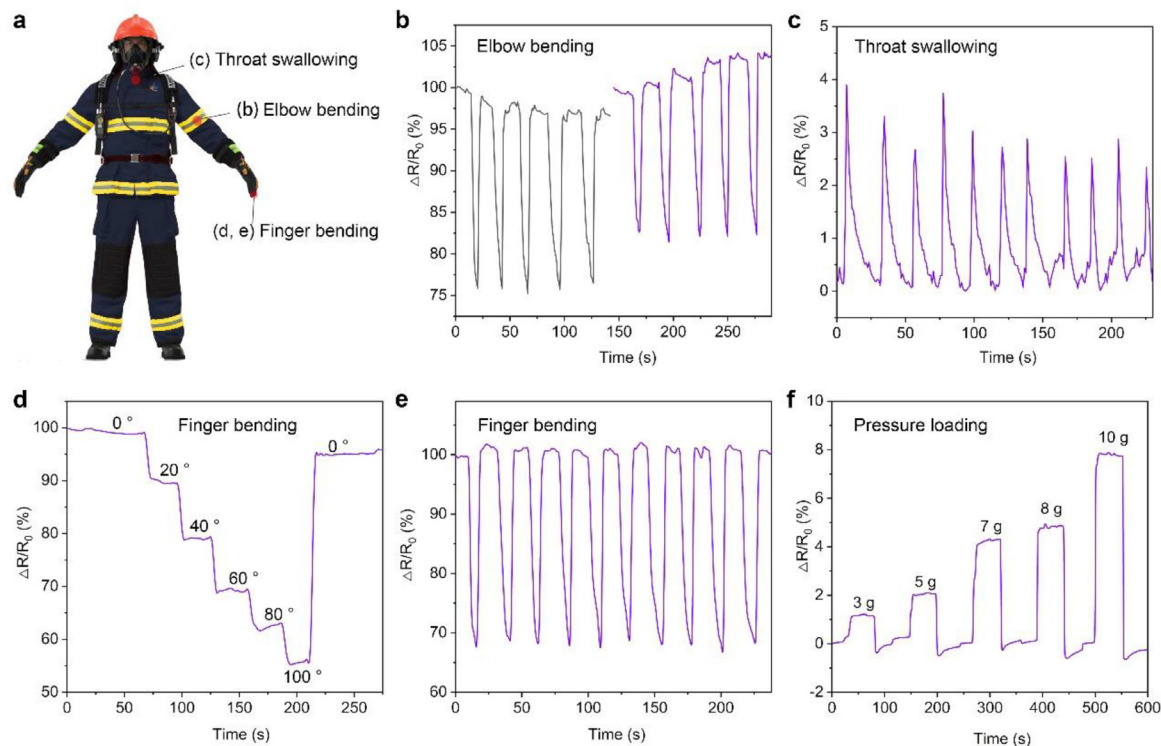


Fig. 6. (a) Schematic diagram of cotton-10BL-Si mounted on different joints for monitoring human motions. (b–e) Responses to elbow bending, throat swallowing, and finger bending, respectively. (f) Response curves of the cotton-10BL-Si under different pressures.

The EMI shielding mechanism of cotton-10BL-Si can be explained as follows: first, the increasing impedance mismatches between shielding fabric and air lead to the immediate reflection of incoming electromagnetic waves before absorption [58]. Second, the absorption of some incoming electromagnetic waves is due to the ohmic loss [58]. Third, the repeated reflection within the porous structure of the shielding fabrics also results in the absorption of electromagnetic waves [59,60]. As a result, only a small proportion of electromagnetic waves transmit through the fabric. It should be pointed out that the  $SE_T$  of cotton-10BL-Si is lower than that of samples FC-5.2Ti<sub>3</sub>C<sub>2</sub>T<sub>x</sub> (31.0 dB) [23] and PTFRF1.2 (35.0 dB) [41] reported in previous work, indicating that the EMI shielding effectiveness of the as-prepared sample is not high enough to meet the requirements of commercial applications (>20 dB).

### 3.3.6. Washability

The silicone elastomer packaged samples are tested according to the AATCC 61-2006 standard to estimate the washability of as-prepared multifunctional cotton fabric. Fig. 5(a) shows the SEM image of cotton-10BL-Si after the wash durability test. Similar to the

sample before washing, the microstructure of the superhydrophobic cotton fabric shows no distinct change with the attachment of irregular particles onto the fiber surface, indicating strong adhesion between the coatings and cotton fabric. As a result, the washed fabrics maintain their original EMI shielding properties. In addition, their LOI values only have slight decreases (< 3%), but still satisfy the application requirements for the flame retardant applications (Fig. 5(b, c)).

### 3.3.7. Motion sensor applications

To verify the suitability of the coated fabric as a human sensor, cotton-10BL-Si is installed in different joints for detecting human motions (Fig. 6(a)). As the average thickness of 10BL-Si coating onto each fibre is  $\sim 4.4 \mu\text{m}$ , the coated fabric can still maintain its good flexibility. For instance, the flexible cotton-10BL-Si can easily deform with a bending angle of  $180^\circ$  (Fig. S6), confirming its good flexibility. As represented in Fig. 6(b), the cotton-10BL-Si is mounted on an elbow to detect bending motions. The repeatable resistance variation signals  $\Delta R/R_0$  demonstrate sensor feedback for repetitive elbow bending [7]. The flexible fabric sensor

shows sensitive and accurate monitoring for slight movements like throat swallowing (Fig. 6(c)). Subsequently, the fabric sensor is attached to a finger to detect signal feedback for different amplitude movements. The results show that the value of  $\Delta R/R_0$  remains stable while the finger bends to a certain angle. And this value rapidly decreases with an increase in bending angle (Fig. 6(d, e)). The outer wall spacing of conductive fibers and the distance between MXene nanosheets will shift under an external force. Therefore, leads to changes in conductive pathway structures and variations in the electrical resistance of the fabrics. When the external force is removed, its resistance can quickly recover. As shown in Fig. 6(f), the fabric sensor exhibits stable responses under five constant loads of 3, 5, 7, 8, and 10 g. As the pressure increases, the MXene layer and conductive fibres are compressed to form tighter contacts, resulting in an increase in the conductive pathways and a decrease in electrical resistance. Therefore, the motion sensor based on Cotton-10BL-Si can meet the practical use of various application scenarios.

#### 4. Conclusion

We have successfully fabricated superhydrophobic, flame-retardant, EMI shielding cotton fabrics in this work. Multiple non-covalent interactions among the composite coatings, including electrostatic interactions of PEI/APP, PEI/MXene, and the chemical bonding of silicone elastomer, are successfully achieved to construct a stable, protective coating on the skeleton of cotton fabrics. Compared to the water permeability of untreated cotton fabric, the PEI-APP-PEI-MXene-Si coating endows fabrics with superhydrophobic features (a CA of  $\sim 152^\circ$ ) and excellent washability. In addition to achieving a high LOI value of 39.5 vol.%, the sample fabric with 10 layers exhibits a desired self-extinguish quality with a UL-94 V-0 rating with 43% and 42% in PHRR and THR, respectively. Furthermore, the high electrical conductivity of the MXene layer allows the coated cotton fabric for EMI shielding applications. Besides its conductivity, the fabric-based pressure sensors and human motion detection sensors also possess stable and regular responses to detect state changes, including throat swallowing, elbow bending, and finger bending. The presented work provides an innovative strategy for developing multifunctional cotton fabrics with flame retardancy, external force sensing, EMI shielding performance, superhydrophobicity, and washability. Therefore, this work presents a suitable alternative in the area textile industry with broad practical application prospects.

#### Acknowledgments

This work was financially supported by the Australian Research Council (Nos. DP190102992, FT190100188), the National Natural Science Foundation of China (No. 51873196), and the Key Research and Development Projects of Zhejiang Province (No. 2019C01098).

#### Supplementary materials

Supplementary material associated with this article can be found, in the online version, at doi:10.1016/j.jmst.2022.05.036.

#### References

- [1] S. Jiang, H. Shao, G. Cao, H. Li, W. Xu, J. Li, J. Fang, X. Wang, *J. Mater. Sci. Technol.* 59 (2020) 92–99.
- [2] S. Liu, S. Qin, Y. Jiang, P. Song, H. Wang, *Compos. Part A-Appl. Sci. Manuf.* 145 (2021) 106376.
- [3] C. Xiong, M. Li, Q. Han, W. Zhao, L. Dai, Y. Ni, *J. Mater. Sci. Technol.* 97 (2022) 190–200.
- [4] J.B. Cheng, H.B. Zhao, A.N. Zhang, Y.Q. Wang, Y.Z. Wang, *J. Mater. Sci. Technol.* 126 (2022) 266–274.
- [5] L. Wang, X. Shi, J. Zhang, Y. Zhang, J. Gu, *J. Mater. Sci. Technol.* 52 (2020) 119–126.
- [6] S.T. Lazar, T.J. Kolibaba, J.C. Grunlan, *Nat. Rev. Mater.* 5 (2020) 259–275.
- [7] M. Zhu, Z. Ma, L. Liu, J. Zhang, S. Huo, P. Song, *J. Mater. Sci. Technol.* 112 (2022) 315–328.
- [8] F. Khan, S. Wang, Z. Ma, A. Ahmed, P. Song, Z. Xu, R. Liu, H. Chi, J. Gu, L.C. Tang, Y. Zhao, *Small Methods* 5 (2021) 2001040.
- [9] X. Cui, Y. Jiang, Z. Xu, M. Xi, Y. Jiang, P. Song, Y. Zhao, H. Wang, *Compos. Part B-Eng.* 211 (2021) 108641.
- [10] G. Malucelli, *Coatings* 6 (2016) 33.
- [11] D. Lin, X. Zeng, H. Li, X. Lai, T. Wu, *J. Colloid Interface Sci.* 533 (2019) 198–206.
- [12] A. Vilcnik, I. Jerman, A. Surca Vuk, M. Kozelj, B. Orel, B. Tomšic, B. Simoncic, J. Kovac, *Langmuir* 25 (2009) 5869–5880.
- [13] G. Rosace, A. Castellano, V. Trovato, G. Iacono, G. Malucelli, *Carbohydr. Polym.* 196 (2018) 348–358.
- [14] Z. Jiang, H. Li, Y. He, Y. Liu, C. Dong, P. Zhu, *Appl. Surf. Sci.* 479 (2019) 765–775.
- [15] L. Xu, W. Wang, D. Yu, *Carbohydr. Polym.* 172 (2017) 275–283.
- [16] T.I. Shaheen, S.S. Salem, S. Zaghoul, *Ind. Eng. Chem. Res.* 58 (2019) 20203–20212.
- [17] F. Fang, X. Zhang, Y. Meng, X. Ding, C. Bao, S. Li, H. Zhang, X. Tian, *Cellulose* 23 (2016) 2161–2172.
- [18] P. Li, B. Wang, Y.Y. Liu, Y.J. Xu, Z.M. Jiang, C.H. Dong, L. Zhang, Y. Liu, P. Zhu, *Carbohydr. Polym.* 237 (2020) 116173.
- [19] W. Wang, J. Guo, X. Liu, H. Li, J. Sun, X. Gu, J. Wang, S. Zhang, W. Li, *Cellulose* 27 (2020) 5377–5389.
- [20] Y. Pan, W. Wang, L. Liu, H. Ge, L. Song, Y. Hu, *Carbohydr. Polym.* 170 (2017) 133–139.
- [21] X. Qiu, Z. Li, X. Li, Z. Zhang, *Chem. Eng. J.* 334 (2018) 108–122.
- [22] X.H. Shi, Y.J. Xu, J.W. Long, Q. Zhao, X.M. Ding, L. Chen, Y.Z. Wang, *Chem. Eng. J.* 353 (2018) 550–558.
- [23] W. Cheng, Y. Zhang, W. Tian, J. Liu, J. Lu, B. Wang, W. Xing, Y. Hu, *Ind. Eng. Chem. Res.* 59 (2020) 14025–14036.
- [24] A. Zhang, H. Zhao, J. Cheng, M. Li, S. Li, M. Cao, Y. Wang, *Chem. Eng. J.* 410 (2021) 128361.
- [25] Y.C. Li, S. Mannen, A.B. Morgan, S. Chang, Y.H. Yang, B. Condon, J.C. Grunlan, *Adv. Mater.* 23 (2011) 3926–3931.
- [26] Z. Ma, X. Liu, X. Xu, L. Liu, B. Yu, C. Maluk, G. Huang, H. Wang, P. Song, *ACS Nano* 15 (2021) 11667–11680.
- [27] Z. Ma, J. Zhang, C. Maluk, Y. Yu, S.M. Seraji, B. Yu, H. Wang, P. Song, *Matter* 5 (2022) 911–932.
- [28] Y. Zhang, Y. Yan, H. Qiu, Z. Ma, K. Ruan, J. Gu, *J. Mater. Sci. Technol.* 103 (2022) 42–49.
- [29] H. Lin, X. Wang, L. Yu, Y. Chen, J. Shi, *Nano Lett.* 17 (2017) 384–391.
- [30] Z.W. Seh, K.D. Fredrickson, B. Anasori, J. Kibsgaard, A.L. Strickler, M.R. Lukatskaya, Y. Gogotsi, T.F. Jaramillo, A. Vojvodic, *ACS Energy Lett.* 1 (2016) 589–594.
- [31] Y. Zhang, Z. Ma, K. Ruan, J. Gu, *Nano Res.* 15 (2022) 5601–5609.
- [32] S. Gong, X. Sheng, X. Li, M. Sheng, H. Wu, X. Lu, J. Qu, *Adv. Funct. Mater.* (2022) 2200570, doi:10.1002/adfm.202200570.
- [33] L. Wang, Z. Ma, Y. Zhang, H. Qiu, K. Ruan, J. Gu, *Carbon Energy* 4 (2022) 200–210.
- [34] Y. Zhang, J. Gu, *Nano Micro Lett.* 14 (2022) 89.
- [35] B. Wang, X. Lai, H. Li, C. Jiang, J. Gao, X. Zeng, *ACS Appl. Mater. Interfaces* 13 (2021) 23020–23029.
- [36] L. Liu, M. Zhu, Z. Ma, X. Xu, S.M. Seraji, B. Yu, Z. Sun, H. Wang, P. Song, *Chem. Eng. J.* 430 (2022) 132712.
- [37] L. Liu, M. Zhu, Y. Shi, X. Xu, Z. Ma, B. Yu, S. Fu, G. Huang, H. Wang, P. Song, *Chem. Eng. J.* 424 (2021) 130338.
- [38] Y. Xue, J. Feng, S. Huo, P. Song, B. Yu, L. Liu, H. Wang, *Chem. Eng. J.* 397 (2020) 125336.
- [39] R. Sun, H.B. Zhang, J. Liu, X. Xie, R. Yang, Y. Li, S. Hong, Z.Z. Yu, *Adv. Funct. Mater.* 27 (2017) 1702807.
- [40] Q. Wang, H. Zhang, J. Liu, S. Zhao, X. Xie, L. Liu, R. Yang, N. Koratkar, Z. Yu, *Adv. Funct. Mater.* 29 (2019) 1806819.
- [41] W. Cheng, Y. Zhang, Y. Tao, J. Lu, J. Liu, B. Wang, L. Song, G. Jie, Y. Hu, *J. Colloid Interface Sci.* 602 (2021) 810–821.
- [42] H.C. Chiang, T.J. Kolibaba, B. Eberle, J.C. Grunlan, *Macromol. Rapid Commun.* 42 (2021) e2000540.
- [43] Y. Shi, M. Sun, C. Liu, L. Fu, Y. Lv, Y. Feng, P. Huang, F. Yang, P. Song, M. Liu, *J. Hazard. Mater.* 423 (2022) 127069.
- [44] D. Xu, S. Wang, Y. Wang, Y. Liu, C. Dong, Z. Jiang, P. Zhu, *Polymers* 12 (2020) 1538.
- [45] C. Liang, Z. Gu, Y. Zhang, Z. Ma, H. Qiu, J. Gu, *Nano Micro Lett.* 13 (2021) 181.
- [46] L. Liu, M. Zhu, Z. Ma, X. Xu, J. Dai, Y. Yu, S. Mohsen Seraji, H. Wang, P. Song, *Chem. Eng. J.* 440 (2022) 135645.
- [47] M. Zhu, L. Liu, Z. Wang, *Compos. Part B-Eng.* 199 (2020) 108283.
- [48] T. Zhang, H. Yan, L. Wang, Z. Fang, *Ind. Eng. Chem. Res.* 52 (2013) 6138–6146.
- [49] J. Alongi, R.A. Carletto, A. Di Blasio, F. Carosio, F. Bosco, G. Malucelli, *J. Mater. Chem. A* 1 (2013) 4779.
- [50] M. Zhu, L. Liu, Z. Wang, *J. Hazard. Mater.* 392 (2020) 122343.
- [51] C. Liu, A. Yao, K. Chen, Y. Shi, Y. Feng, P. Zhang, F. Yang, M. Liu, Z. Chen, *Compos. Part B-Eng.* 226 (2021) 109363.
- [52] C. Liu, K. Xu, Y. Shi, J. Wang, S. Ma, Y. Feng, Y. Lv, F. Yang, M. Liu, P. Song, *Mater. Today Phys.* 22 (2022) 100607.
- [53] Y. Xue, J. Feng, Z. Ma, L. Liu, Y. Zhang, J. Dai, Z. Xu, S. Bourbigot, H. Wang, *P. Song, Mater. Today Phys.* 21 (2021) 100568.
- [54] J. Feng, Z. Ma, Z. Xu, H. Xie, Y. Lu, C. Maluk, P. Song, S. Bourbigot, H. Wang, *Chem. Eng. J.* 431 (2022) 134259.

- [55] S. Huang, L. Wang, Y. Li, C. Liang, J. Zhang, *J. Appl. Polym. Sci.* 138 (2021) 50649.
- [56] C. Liu, W. Wu, Y. Shi, F. Yang, M. Liu, Z. Chen, B. Yu, Y. Feng, *Compos. Part B-Eng.* 203 (2020) 108486.
- [57] Y. Zhang, K. Ruan, X. Shi, H. Qiu, Y. Pan, Y. Yan, J. Gu, *Carbon* 175 (2021) 271–280.
- [58] X. Wang, Z. Lei, X. Ma, G. He, T. Xu, J. Tan, L. Wang, X. Zhang, L. Qu, X. Zhang, *Chem. Eng. J.* 430 (2022) 132605.
- [59] Z. Ma, X. Xiang, L. Shao, Y. Zhang, J. Gu, *Angew. Chem. Int. Ed.* 61 (2022) e202200705.
- [60] T. Tang, S. Wang, Y. Jiang, Z. Xu, Y. Chen, T. Peng, F. Khan, J. Feng, P. Song, Y. Zhao, *J. Mater. Sci. Technol.* 111 (2022) 66–75.